Supporting Information

Bimetallic oxyhydroxide in situ derived from Fe_2Co-MOF for efficient electrocatalytic oxygen evolution

Xintong Ling, [†ac] Feng Du, [†e] Yintong Zhang,[ac] Yan Shen,[cf] Wa Gao,[ac] Zhiyuan Wang,[h] Guoling Li,*[gh] Bo Zhou,[g] Tao Li,*[b] Qing Shen,[i] Yujie Xiong,[j] Xiaoyong Wang,[ac] Yong Zhou,*[acd] and Zhigang Zou.[acd]

[a]*School of Physics, National Laboratory of Solid State Microstructures, Nanjing University, Nanjing, Jiangsu 210093, P. R. China.*

[b]*School of Chemistry and Pharmaceutical Engineering, Nanyang Normal University, Nanyang, Henan 473061, P. R. China.*

[c]*Jiangsu Key Laboratory for Nano Technology, Nanjing University, Nanjing, Jiangsu 210093, P. R. China. E-mail: zhouyong1999@nju.edu.cn.*

[d]*School of Science and Engineering, The Chinese University of Hong Kong, Shenzhen, Guangdong 518172, P. R. China.*

[e]*Institute of Materials Science and Devices, School of materials science and Engineering, Suzhou Univer sity of Science and Technology, Suzhou 215009, P. R. China.*

[f]*College of Engineering and Applied Sciences, Nanjing University, Nanjing 210093, P. R. China.*

[g]*Chemistry and Chemical Engineering Guangdong Laboratory, Shantou 515031, China.*

[h]*School of Physics and Engineering, Henan University of Science and Technology, Luoyang 471023, China*

[i]*University of Electro Communication, Graduate school of Informatics and Engineering, 1-5-1 Chofugaoka, Chofu, Tokyo, 182-8585, Japan*

[j]*Hefei National Laboratory for Physical Sciences at the Microscale, School of Chemistry and Materials S cience, University of Science and Technology of China, Hefei,*
230026, PR China

† Ling and Du contributed equally to this work

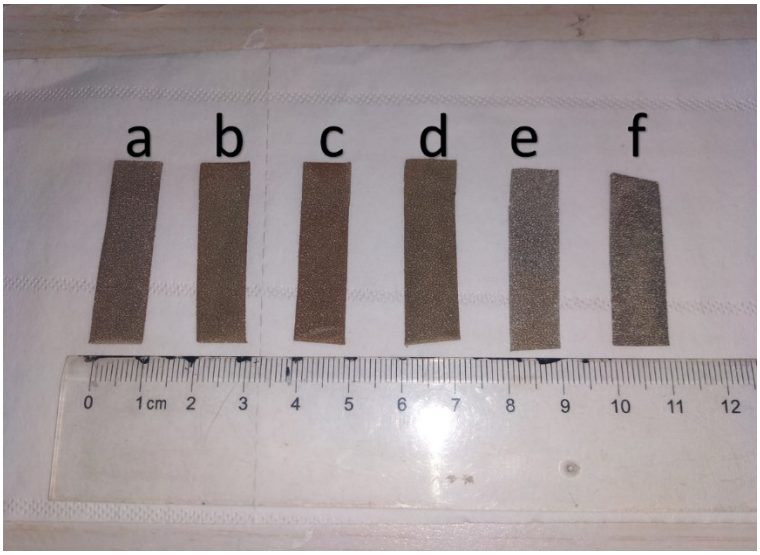

Fig. S1 Photos of Co MOF/NF, Fe MOF/NF, and Fe-Co MOF/NFs on nickel foams: (a) Co MOF/NF, (b) Fe: Co= 3: 7, (c) Fe: Co=5: 5, (d) Fe: Co= 7: 3, (e) Fe: Co= 9: 1, and (f) Fe MOF/NF.

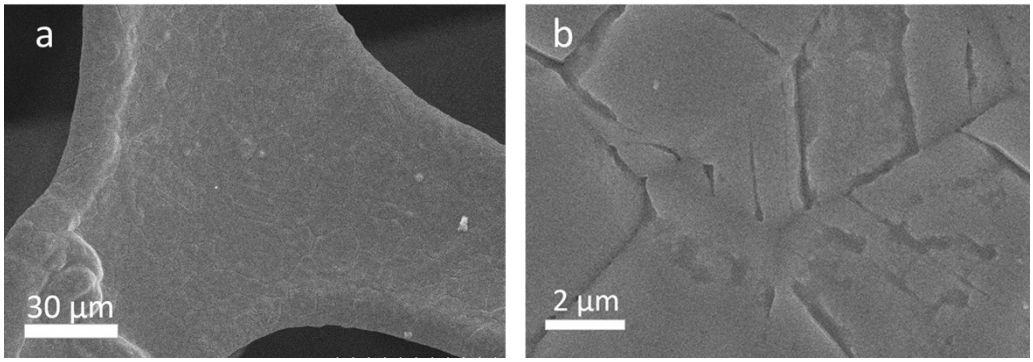

Fig. S2 SEM images of nickel foam (a, b).

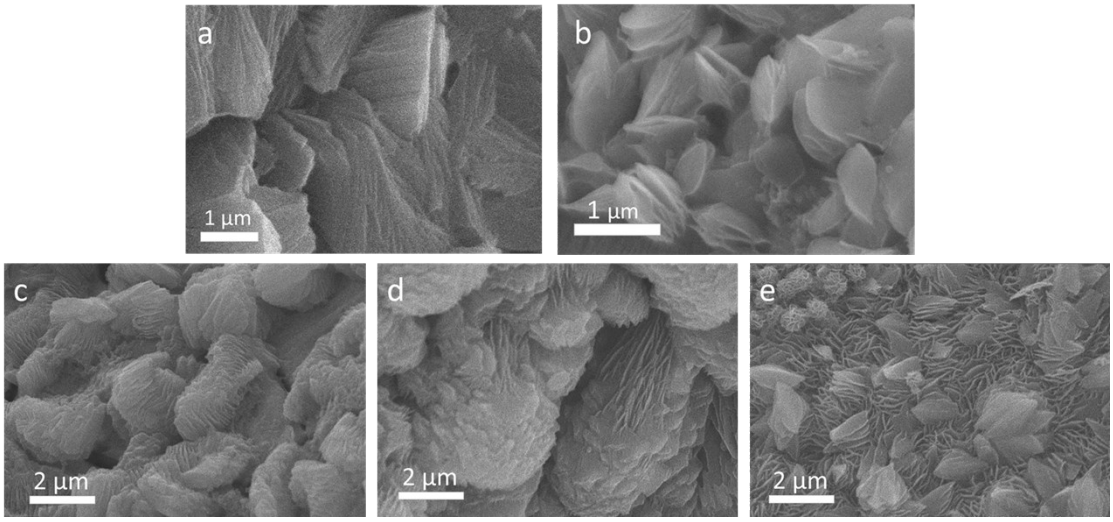

Fig. S3 SEM images of (a) Co MOF/NF, (b) Fe MOF/NF, Fe-Co MOF/NF of (c) Fe: Co= 3: 7, (d) Fe: Co= 5: 5, and (e) Fe: Co = 9: 1.

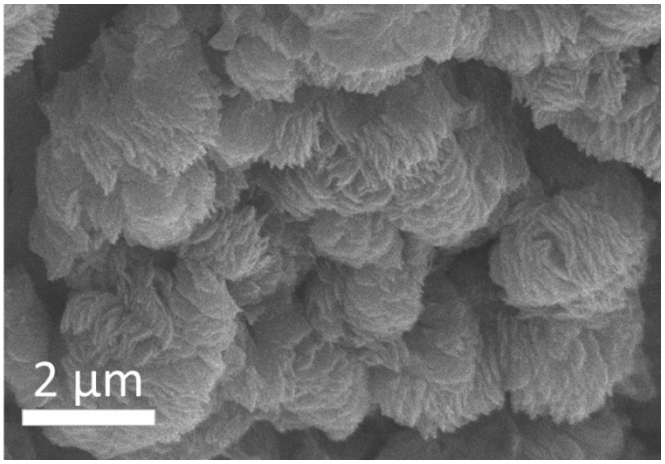

Fig. S4 SEM image of Fe-Co MOF/NF (Fe: Co= 7: 3) after stability test.

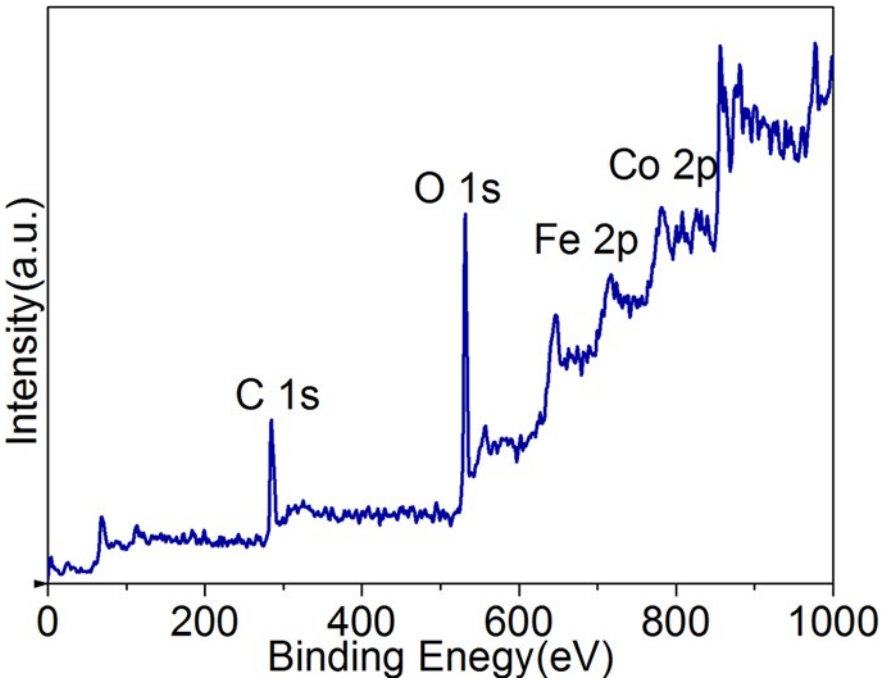

Fig. S5 XPS spectra of Fe-Co MOF/NF (Fe: Co= 7: 3).

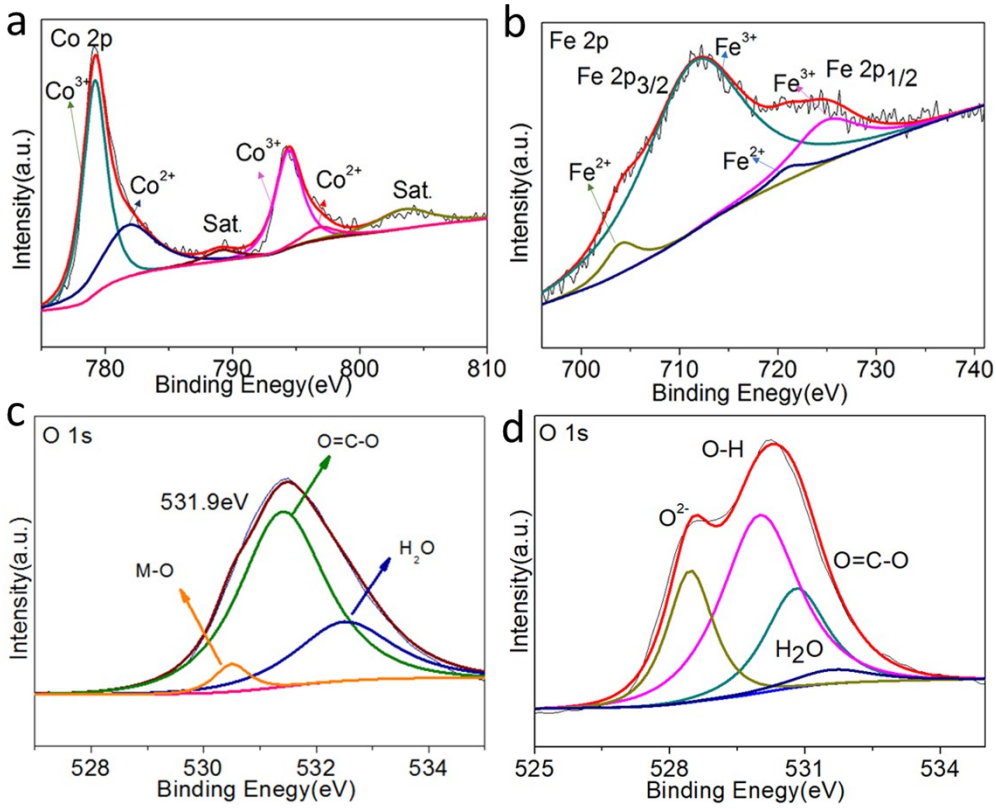

Fig. S6 The XPS spectra of (a) Co 2p and (b) Fe 2p for Fe-Co MOF/NF (Fe: Co= 7: 3) after OER test. XPS spectra of O 1s for Fe-Co MOF/NF (Fe: Co= 7: 3) (c) before OER test and (d) after OER test.

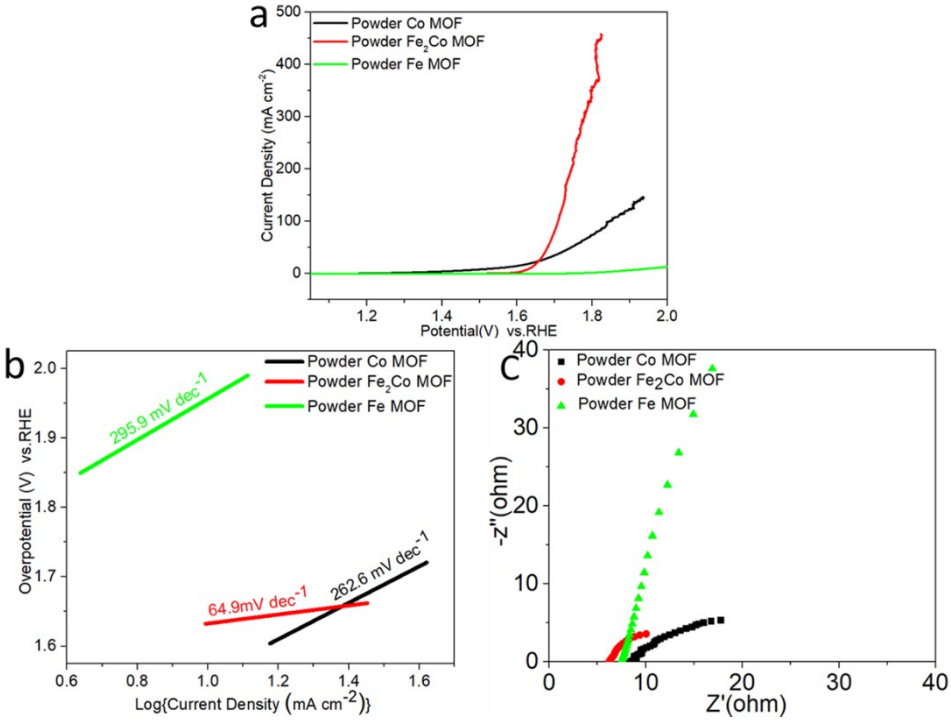

Fig. S7 (a) LSV curves, (b) Tafel plots, and (c) Nyquist plots of Co MOF, Fe MOF, and Fe_2Co MOF on the GC.

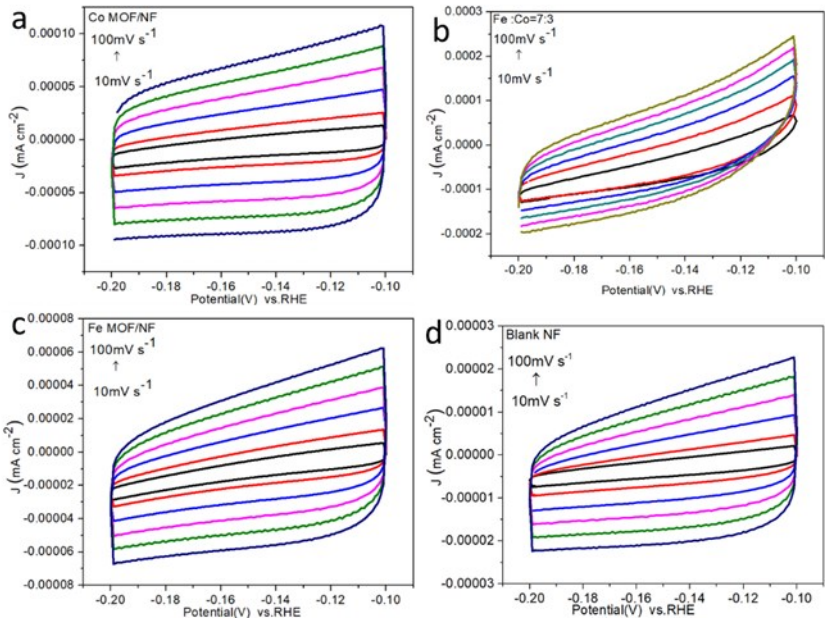

Fig. S8 CVs measured in a non-Faradaic region of (a) Co MOF/NF, (b) Fe-Co MOF/NF (Fe: Co= 7: 3), (c) Fe MOF/NF, and (d) blank NF.

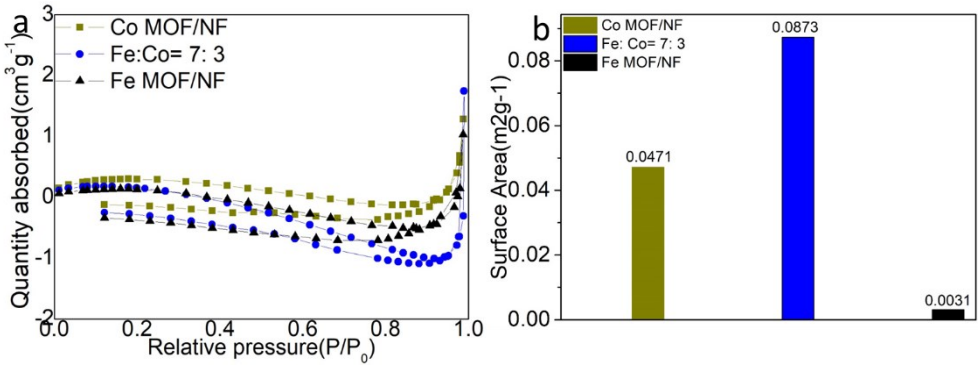

Fig. S9 (a) Nitrogen adsorption-desorption isotherms of Co MOF/NF, Fe MOF/NF and Fe-Co MOF/NF (Fe: Co= 7: 3). (b) BET surface area values of Co MOF/NF, Fe MOF/NF and Fe-Co MOF/NF (Fe: Co= 7: 3).

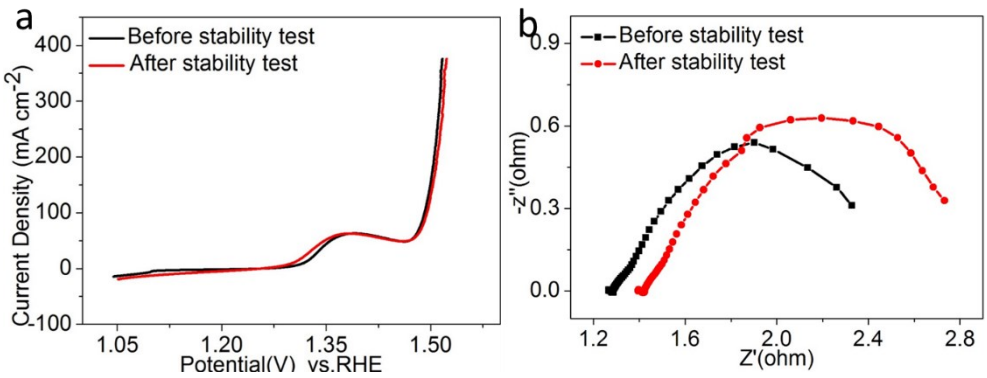

Fig. S10 (a) LSV curves and (b) Nyquist plots of Fe-Co MOF/NF (Fe: Co= 7: 3) before and after stability test.

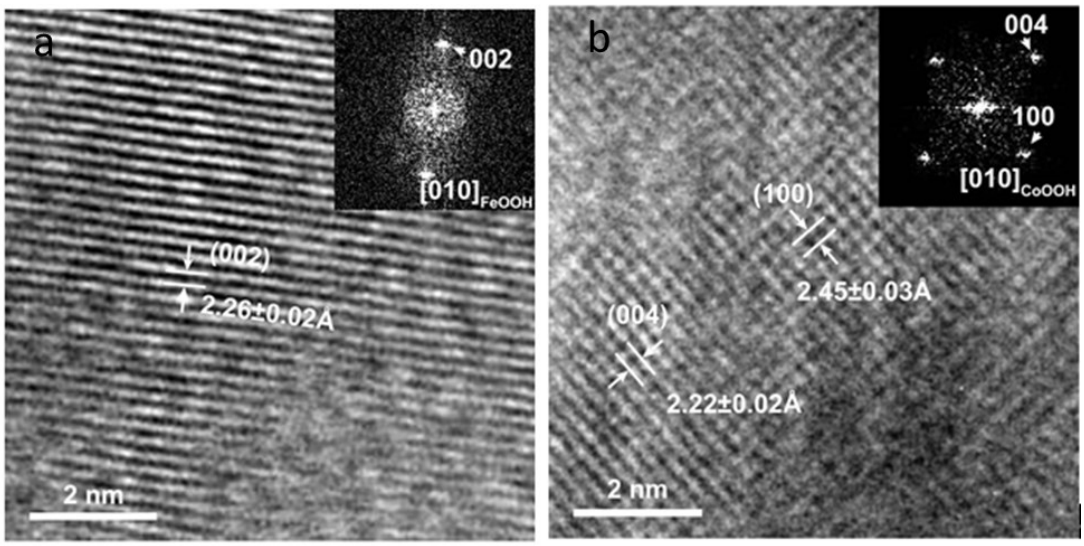

Fig. S11 The HRTEM images of (a) Fe MOF/NF and (b) Co MOF/NF after OER test. (Inset of a and b): SAED pattern of Fe MOF/NF and Co MOF/NF after OER test.

Table. S1 MOF labels and stoichiometry of synthesis are provided.

Catalyst	$CoCl_2 \bullet 6H_2O$ (mmol)	$Fe(NO)_3 \bullet 9H_2O$ (mmol)	TPA (mmol)
Co MOF/NF	1	0	1
Fe: Co= 3: 7	0.7	0.3	1
Fe: Co= 5: 5	0.5	0.5	1
Fe: Co= 7: 3	0.3	0.7	1
Fe: Co= 9: 1	0.1	0.9	1
Fe MOF/NF	0	1	1

Table. S2 OER performances for Fe MOF/NF, Co MOF/NF, Fe-Co MOF/NFs with varying Fe/Co batch ratios (Fe: Co= 9: 1, Fe: Co= 7: 3, Fe: Co= 5: 5, and Fe: Co= 3: 7), and blank NF.

Catalysts	Overpotential (10 mA cm^{-2})	Tafel slope
Fe MOF/NF	257 mV	69.1 mV dec^{-1}
Fe: Co= 9: 1	236 mV	63.8 mV dec^{-1}
Fe: Co= 7: 3	224 mV	45.3 mV dec^{-1}
Fe: Co= 5: 5	253 mV	52.9 mV dec^{-1}
Fe: Co= 3: 7	289 mV	53.2 mV dec^{-1}
Co MOF/NF	289 mV	61.6 mV dec−1
blank NF	436 mV	175.6 mV dec^{-1}

Table. S3 Comparison of OER performance with other reported non-precious electrocatalysts.

Entry	Catalyst	Overpotential (mV @mA cm^{-2})	Tafel slope (mV dec^{-1})	reference
1	Fe_2Co MOF/NF	224@10	45	This work
2	Fe_2Co MOF/GC	400@10	65	This work
3	MIL-53(Co-Fe)/NF	262@100	69	1
4	CoFe-MOF-OH NF	265@10	44	2
5	Co-Fe NPs	369@20	51	3
6	Co_2Fe-MOF	280@10	45	4
7	$Co_{0.6}Fe_{0.4}$-MOF-74	280@10	56	5
8	CoFe-UMNs	290@10	31	6
9	NiCo/Fe_3O_4/MOF-74	238@10	29	7
10	CoNi(1:1)-MOF	265@10	56	8
11	NiFe-MOF	240@10	34	9
12	NiCo-UMOFNs	250@10	42	10

Table. S4 Free energies of adsorption. This table shows the free energies of adsorption for OH*, O* and OOH*, GOER and for oxygen evolution via the AEM pathway at the top Fe/Co active sites on FeOOH (010), $Fe_{0.67}Co_{0.33}OOH$ (010) and CoOOH (010).

Electrocatalyst	Active site	ΔG_{OH} (eV)	ΔG_{O} (eV)	ΔG_{OOH} (eV)	ΔG^{OER} (eV)
FeOOH	Fe-top	1.21	2.70	4.21	1.51
$Fe_{0.67}Co_{0.33}OOH$	Fe-top	0.98	2.55	4.08	1.57
$Fe_{0.67}Co_{0.33}OOH$	Co-top	0.73	2.83	3.74	2.10
CoOOH	Co-top	1.04	2.52	4.32	1.80

Table. S5 Free energies of adsorption. This table shows the free energies of adsorption for OH*, O* and OOH*, ΔG^{OER} and Δ for oxygen evolution via the LOM pathway at the bridge Fe-Fe or Fe-Co active sites on FeOOH (010) and $Fe_{0.67}Co_{0.33}OOH$ (010) with an OLHL vacancy.

Electrocatalyst	Active site	ΔG_{OH} (eV)	ΔG_{O} (eV)	ΔG_{OOH} (eV)	ΔG^{OER} (eV)
FeOOH	Fe-Fe-bridge	-0.21	1.36	3.04	1.88
$Fe_{0.67}Co_{0.33}OOH$	Fe-Fe-bridge	-0.08	1.51	3.19	1.73
$Fe_{0.67}Co_{0.33}OOH$	Fe-Co-bridge	-0.15	1.06	3.06	2.00

Table. S6 Bader charges in the elementary charge e for Fe and Co cations in the bulk and at the (010) surfaces of FeOOH, $Fe_{0.67}Co_{0.33}OOH$ and CoOOH.

Electrocatalyst	bulk		(010)		(010) with an OH vacancy	
	Fe	Co	Fe	Co	Fe	Co
FeOOH	+1.28	---	+1.32	---	+1.18	---
$Fe_{0.67}Co_{0.33}OOH$	+1.32	+1.17	+1.14	+1.21	+1.12	+1.22
CoOOH	---	+1.26	---	+0.89	---	---

Computational details:

Density functional theory (DFT) calculations are done using the projector-augmented wave method and a plane-wave basis set as implemented in the Vienna Ab initio Simulation Package (VASP).[11, 12] The valence configurations are treated as $1s^1$ for H, $2s^22p^4$ for O, $3d^74s^1$ for Fe, and $3d^84s^1$ for Co. To better describe the Fe 3*d* and Co 3*d* electrons, the effective *U* values of 5.30 eV and 3.32 eV are applied in the Hubbard model (DFT+*U*), respectively. The Bayesian Error Estimation Functional with van der Waals correlation (BEEF–vdW) is employed.[13] The cutoff energy for plane-wave basis functions is 550 eV. Since The bulk lattice parameters of the transition metal oxyhydroxides are fully optimized based on experimental data (FeOOH: PDF#13-0087, a=b= 2.941 Å, c= 4.49 Å, γ= 120°; CoOOH: PDF#26-1107, a=b= 2.855 Å, c= 8.805 Å, γ= 120°). By substituting a Fe atom with a Co atom within the 3×1×1 supercell of FeOOH, we obtain the bulk structure of $Fe_{0.67}Co_{0.33}OOH$. Based on the optimized structural parameters, we construct periodic surface slabs with five Fe/Co layers separated by at least 14 Å of vacuum for the (010) surfaces of FeOOH, $Fe_{0.67}Co_{0.33}OOH$, and CoOOH. Atomic positions within the top three layers of the slabs are allowed to relax in OH*, O* and OOH* binding energy calculations. All calculations are done in Γ-centered Monkhorst–Pack *k*-point meshes with a reciprocal-space resolution of 0.15 $Å^{-1}$. The energy convergence is 10^{-5} eV and the force convergence 0.02 eV/Å.

As is known, the catalytic activity of the material is determined by the binding energies of the reaction intermediates to the active sites of the catalyst. In the oxygen evolution reaction via the adsorbate evolution mechanism (AEM) pathway, OH*, O* and OOH* intermediates are involved. To estimate the adsorption free energies ΔG of different intermediate at zero potential and pH = 0, we calculate the binding energies ΔE of each intermediate and corrected them with zero-point energy (ZPE) and entropy (TS) using $\Delta G = \Delta E + \Delta ZPE - T\Delta S$.[14] Here, we use the computational hydrogen electrode (CHE) model, which exploits that the chemical potential of a proton-electron pair is equal to gas-phase H_2 at standard conditions. As the ground state of the O_2 is poorly described in DFT calculations we use gas-phase H_2O and H_2 as reference states as they are readily treated in the DFT calculations. The entropy for H_2O is calculated at 0.035 bar which is the equilibrium pressure of H_2O at 300 K.

The free energy of this state is therefore equal to that of liquid water.[14] In the oxygen evolution reaction, the limiting potential is related to the highest free energy step ΔG^{OER} = Max($\Delta G_{OH*}-\Delta G_{H2O(l)}$), ($\Delta G_{O*}-\Delta G_{OH*}$), ($\Delta G_{OOH*}-\Delta G_{O*}$), ($\Delta G_{O2(g)}-\Delta G_{OOH*}$).[15]

In the oxygen evolution reaction via the lattice oxhydryl oxidation mechanism (LOM) pathway, O_L*, O_LOH* and O_LH_L* intermediates are involved. Here * denotes the Fe-Fe or Fe-Co bridge site where the lattice oxhydryl O_LH_L locates, and the subscript L indicates the lattice. If we make a vacancy of the lattice oxhydryl O_LH_L on the FeOOH (010) or $Fe_{0.67}Co_{0.33}OOH$ (010) surface, then we could reproduce the four electrochemical steps in the AEM pathway to simulate those in the LOM pathway. We should keep in mind that the first electrochemical step in the LOM pathway is the deprotonation of O_LH_L* rather than the adsorption of OH* in the AEM pathway.

In addition, the hydroxyl vacancy formation energy is calculated via $E_f = E(*) + E(H_2O) - E(OH*) - 1/2E(H_2)$ according to $OH* + 1/2H_2 \rightarrow * + H_2O$.

References

1 M. W. Xie, Y. Ma, D. M. Lin, C. G. Xu, F. Y. Xie, and W. Zeng, *Nanoscale*. 2020, **12**,67.

2 Z. H. Zou, T. T. Wang, X. H. Zhao, W. J. Jiang, H. R. Pan, D. Q. Gao, and C. L. Xu. *ACS Catal*. 2019, **9**,7356−7364.

3 W. Adamson, X. Bo, Y. b. Li, B. H.R. Suryanto, X. J. Chen, C. Zhao. *Catalysis Today*. 2020, **351**, 44–49.

4 S. L. Xie, F. Li, S. X. Xu, J.Y. Li, W. Zeng. *Chinese Journal of Catalysis*. 2019, **40**, 1205–1211

5 X. H. Zhao, B. Pattengale, D. H. Fan, Z. H. Zou, Y. Q. Zhao, J. Du, J. E. Huang, C. L. Xu. *ACS Energy Lett*. 2018, **3** 2520−2526.

6 G. T. Hai, X. L. Jia, K. Y. Zhang, X. Liu, Z. Y. Wu, G. Wang. *Nano energy*. 2018, **44**, 345-352.

7 X. L. Wang, H. Xiao, A. Li, Z. Li, S. J. Liu, Q. H. Zhang, Y. Gong, L. R. Zheng, Y. Q. Zhu, C. Chen, D. S. Wang, Q. Peng, Lin Gu, X. D. Han, J. Li, and Y. D. Li, *J. Am. Chem. Soc*. 2018, **140**, 15336−15341.

8 M. J. Liu, W. R. Zheng, S. J. Ran, S. T. Boles, and L. Y. S. Lee, Adv. Mater. *Interfaces*. 2018, **5**, 1800849.

9 J. Duan, S. Chen, and C. Zhao, *Nat. Commun*. 2017, **8**,15341–15348.

10 S. Zhao, Y. Wang, J. Dong, C.-T. He, H. Yin, P. An, K. Zhao, X. Zhang, C. Gao, L. Zhang, J. Lv, J. Wang, J. Zhang, A. M. Khattak, N. A. Khan, Z. Wei, J. Zhang, S. Liu, H. Zhao, and Z. Tang, *Nat. Energy*. 2016, **1**, 16184–16194.

11 P.E. Blöchl, *Phys. Rev. B*. 1994, **50** , 17953–17979.

12 G. Kresse & J. Furthmüller, *Phys. Rev. B*. 1996, **54**, 11169–11186.

13 J. Wellendorff, K. T. Lundgaard, A. Møgelhøj, V. Petzold, D. D. Landis, J. K. Nørskov, T. Bligaard & K.W. Jacobsen, *Phys Rev B*. 2012, **85**,235149 .

14 J. K. Norskov, J. Rossmeisl, A. Logadottir, L. Lindqvist, J. R. Kitchin, T. Bligaard & H. Jonsson, *J. Phys. Chem. B*. 2004, **108**, 17886-17892.

15 M. García-Mota, A. Vojvodic, H. Metiu, I.C. Man, H. Y. Su, J. Rossmeisl & J. K. Nørskov, *ChemCatChem*. 2011, **3**, 1607- 1611.